Estimation of human impedance and motion intention for constrained human-robot interaction

Article (Accepted Version)

Estimation of Human Impedance and Motion Intention for Constrained Human-Robot Interaction

Xinbo Yu[1,2,3], Yanan Li[4], Shuang Zhang[1,2,3*], Chengqian Xue[1,2,3], Yu Wang[5]

1. School of Automation and Electrical Engineering, University of Science and Technology Beijing, Beijing 100083*, China.*

2. Institute of Artificial Intelligence, University of Science and Technology Beijing, Beijing 100083*, China.*

3. Key Laboratory of Knowledge Automation for Industrial Processes, Ministry of Education, University of Science and Technology Beijing, Beijing 100083*, China.*

4. Department of Engineering and Design, University of Sussex, Brighton BN1 9RH*, UK.*

5. Institute of Automation, Chinese Academy of Sciences, Beijing 100190*, China.*

Abstract– In this paper, a complete framework for safe and efficient physical human-robot interaction (pHRI) is developed for robot by considering both issues of adaptation to the human partner and ensuring the motion constraints during the interaction. We consider the robot's learning of not only human motion intention, but also the human impedance. We employ radial basis function neural networks (RBFNNs) to estimate human motion intention in real time, and least square method is utilized in robot learning of human impedance. When robot has learned the impedance information about human, it can adjust its desired impedance parameters by a simple tuning law for operative compliance. An adaptive impedance control integrated with RBFNNs and full-state constraints is also proposed in our work. We employ RBFNNs to compensate for uncertainties in the dynamics model of robot and barrier Lyapunov functions are chosen to ensure that full-state constraints are not violated in pHRI. Results in simulations and experiments show the better performance of our proposed framework compared with traditional methods.

Index Terms —- Human motion intention estimation, impedance learning, adaptive neural network control, full-state constraints, barrier Lyapunov functions.

I. Introduction

Robots are coming to our daily lives driven by social needs and development of robotics, intelligent control and machine learning [1]. Relying on complementary advantages of humans' perception and

*Corresponding author is Shuang Zhang. E-mail: zhangshuang.ac@gmail.com

robots' execution capabilities, various tasks can be accomplished by cooperative efforts of human and robot. Physical human-robot interaction (pHRI) occurs in human robot collaborative tasks such as neuro-rehabilitation, object transportation [2] and so on.

In human robot collaborative tasks, it is essential that robots acquire force information by force or torque sensor and respond to humans in a proper way [3]. Force control is a well-developed interaction control strategy but limited by poor robustness against disturbances [4]. Hybrid position/force control is widely utilized in pHRI, but interaction forces are deemed as disturbances [5]. In [6], a compliance selection vector is employed in proposed controller to determine whether the system is under position or force control. However, the controller makes the interaction unstable when robot interacts with a stiff environment, and brings sluggish response in interaction with a soft environment. Due to robustness and feasibility, impedance control is widely used to relate interactive force with deviations from desired positions [7]. In [8], a position-based impedance control is developed where there are two control loops. In this controller, the output of outer loop is a virtual desired trajectory, and the control objective of inner loop is to track the virtual desired trajectory, so if tracking errors converge to zero, the robot will perform a desired impedance.

How a robot detects what the human is trying to do poses many challenges in HRI. If robots have no knowledge of human motion intention, they may become additional loads for human. Conversely, if robots know human motion intention, robots can be initiative to move actively, and human will cost less effort to guide robots. Therefore, how to estimate motion intention of human partners attracts substantial attention of researchers. In [9], human motion intention is estimated and it enables a robot to follow human for fast point-to-point tasks. Without force sensors, changes in control effort are utilized to obtain the estimation of human motion intention in [10]. In [11], intentional reaching direction is defined for describing the human's upper limb motion intention in real time in exoskeleton. In [12], a walk intention estimation method is proposed for an omnidirectional cane robot. Human motion intention has different definitions in literatures. In [13], human motion intention is defined as human's current position which is provided with the feedback by a multi-modal interface. In [14], human motion intention is defined as target position or time-varying desired trajectory which is estimated by online neural networks (NNs) based on available sensory information.

How to make robot adjust its desired impedance according to the environments' impedance [15] or humans' impedance [16] is also a key issue in pHRI. In [17], authors propose an impedance learning method for a robot to interact with an unknown environment to avoid large interaction forces. Some

learning methods have been utilized in literatures [18]. Reinforcement learning, which adopts an actor-critic algorithm, is utilized in [19] to acquire optimal impedance parameters of robot for contact tasks. NNs are also trained in [20] by using an iterative method to regulate stiffness and viscosity parameters. Probabilistic methods are also employed in impedance learning. In [21], a human arm impedance estimation method is proposed for a 2-DOF assembly robot subject to nonlinear frictions. In [22], virtual stiffness can be estimated by the weight least-squares estimation, and it is included in the complete set of task-parameterized Gaussian mixture model. To our best knowledge, there are no works that combine human motion intention estimation and impedance learning.

Various control strategies have been developed to address uncertainties in dynamics, such as adaptive control strategies, optimal control [23], [24], fault-tolerant control [25], boundary control [26] and finite-time tracking control [27]. Radial basis function neural networks (RBFNNs) are used to compensate for unknown dynamic uncertainties in [28], and also utilized in bimanual dual arm robots [29], underactuated wheeled robots [30], flapping wing aerial vehicles [31], underwater robots [32], biped robots [33], flexible robots [34], gantry cranes [35], marine surface vessels [36], soft robots [37] and autonomous underwater vehicles [38]. Disturbance observer is also designed combined with NNs to estimate uncertain disturbances in literatures [39]. In [40], adaptive NN controllers integrating nonlinear disturbance observer are proposed in designing a human upper arm exoskeleton. In [39], a disturbance observer is proposed in robust tracking control for self-balancing mobile robots. State observer is also designed to obtain unknown system states for uncertain systems [41] and unmodeled nonlinear systems [42]. In our work, we utilize RBFNN to compensate for uncertainties in dynamic model of robot.

Furthermore, safety is extremely important in situations where human directly interacts with robots [43]. In this sense, constrained robots have drawn much attention of researchers [44], such as input constraint [45], [46] and output constraint [47]. Using barrier Lyapunov functions (BLFs) is an effective method to make robots take into account motion constraints, such as position constraints and velocity constraints in joint space or Cartesian space. In [48], output constraints based on BLFs are introduced into controller for nonlinear systems and constraints are guaranteed not to be transgressed. In [49], output constraints are considered to be time-varying, and constraint satisfaction is ensured by constructing proper BLFs. In [50], log-type BLFs are designed to avoid the violation of output constraints with full-state feedback control. In [51], force/motion control is designed for a mobile robotic manipulator with uncertain holonomic constraints. In our paper, full-state constraints based on log-type BLFs are considered for constraining position and velocity in human robot collaborative tasks.

Based on above discussions, to our best knowledge no works propose integrated methods considering human motion intention estimation and impedance learning. Therefore, in this paper we consider robot's learning of not only human motion intention, but also human impedance. An adaptive impedance control integrated with NNs and motion constraints is proposed for robots collaborating with human to perform human-robot collaborative tasks. The main contributions of our work include:

1) Different from existing works in the field of pHRI, we estimate both impedance parameters and motion intention of human partner, so that the robot can collaborate with human partner to perform tasks actively.
2) We propose NNs to compensate for uncertainties in dynamic model of robot which improves tracking accuracy. Impedance controller design and stability analysis are conducted rigorously.
3) Full-state constraints are considered in the controller design to avoid collision and violation of speed limit. In this sense, a complete framework for safe and efficient human-robot interaction is developed for robot by considering both issues of adaptation to the human partner and ensuring the motion constraints during the interaction.

Our work is structured as follows: in Section II, the dynamic models of robot and human are analysed, and the control objective is introduced; in Section III, we analyse the human motion intention estimation method based on RBFNNs, while impedance learning is developed afterwards, and then an adaptive position-based impedance control strategy is considered subject to full-state constraints, with RBFNNs also utilized to compensate for uncertainties in robot's dynamic model to improve tracking accuracy when robot tracks the virtual desired trajectory in the inner control loop; in Section IV, the simulation results show the effectiveness of our proposed framework; in Section V, an experiment on a Baxter robot is designed to evaluate the performance of our controller; in Section VI, conclusion of the paper is given.

II. System Description

We consider a human robot collaborative task as shown in Fig. 1, where a human partner collaborates with robot to carry out an object transporting task. In this task, compliant cooperation should be ensured for reducing human effort. Position and velocity of robot should be restricted for safe cooperation. In this section, we firstly describe the dynamic model of both robot and human.

A. Dynamic Model

I. Dynamic Model of Robot

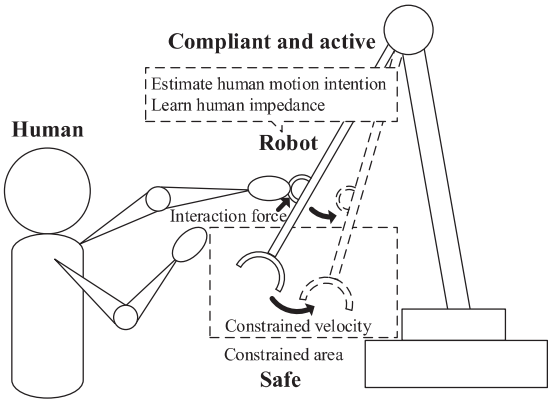

(a) compliant and safe pHRI.

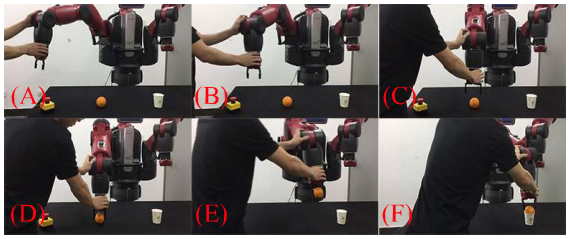

(b) object transporting task by human and Baxter robot.

Fig. 1: Object transporting scenarios.

The dynamic model of robot in the task space is described as follows:

$$M_t(x)\ddot{x} + C_t(x,\dot{x})\dot{x} + G_t(x) = u + f, \tag{1}$$

where $x \in \mathbb{R}^n$ represents position vector, $\dot{x} \in \mathbb{R}^n$ represents velocity vector, $\ddot{x} \in \mathbb{R}^n$ represents acceleration vector. $M_t(x) \in \mathbb{R}^{n\times n}$, $C_t(x,\dot{x})\dot{x} \in \mathbb{R}^n$ and $G_t(x) \in \mathbb{R}^n$ denote the inertia matrix, Coriolis and centripetal force vector and gravitational force vector, respectively. $u \in \mathbb{R}^n$ and $f \in \mathbb{R}^n$ denote control force vector of robot and interaction force vector between human and robot, respectively. The dynamic model of robot in joint space is given in *Appendix A*.

II. Dynamic Model of Human

In object transporting tasks, interaction force is exerted on the robot by human arm. Therefore, it is essential to study the dynamic model of the human arm. In this paper, we suppose that the dynamics of human arm are described by the following damping-stiffness model:

$$f = -D_h\dot{x} + K_h(x_d - x), \tag{2}$$

where D_h and K_h denote damper and stiffness matrices of human, respectively. x_d denotes the human motion intention. In our paper, human impedance D_h and K_h can be time-varying or constant, and x_d is time-varying.

Remark 1: The human's dynamic model (2) is a simplified model, as discussed and verified in [52]: the damper and stiffness matrices usually dominate the model of human arm, so the mass matrix is ignored.

B. Control Objective

Position-based impedance control structure is employed in our work. Firstly, we consider a target impedance model for robot as follows:

$$f = D_d(\dot{\hat{x}}_d - \dot{x}_r) + K_d(\hat{x}_d - x_r), \tag{3}$$

where D_d and K_d denote the desired damper and stiffness matrices respectively, x_r is the virtual desired trajectory, and $\hat{x}_d$ denotes the estimated human motion intention. The control structure is proposed in Fig. 2. Seen from Fig. 2, when tracking control design is effective to ensure x tracking x_r, we rewrite the impedance model (3) as follows:

$$f = D_d(\dot{\hat{x}}_d - \dot{x}) + K_d(\hat{x}_d - x). \tag{4}$$

As discussed before, human is leading the task and he/she has the knowledge of the target position or

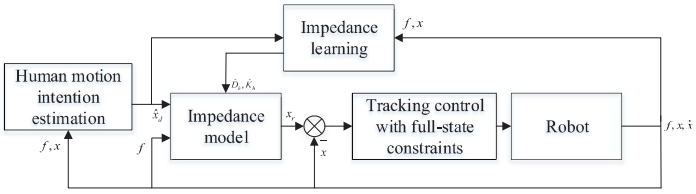

Fig. 2: Control architecture.

desired trajectory, and the robot will follow the human motion. If the robot does not know the human motion intention, i.e., x_d may be far away from x in (2), human will cost more effort to operate the robot due to a significant interaction force f, but if the robot knows the human motion intention x_d and changes $\hat{x}_d$ accordingly, the human partner will move the robot easily because the interaction force in (2) is less. Therefore, firstly we will propose an estimation method to obtain the human motion intention.

When human plays an active role to move robot in pHRI, it would be desirable that the robot is able to reduce its desired impedance parameters in (4) to make it compliant. Conversely, if human is not willing

to lead tasks, robot should increase the impedance parameters to ensure the positioning accuracy subject to external disturbances. Inspired by this idea, we suppose that impedance matrices D_d, K_d, D_h, K_h are diagonal, and design an impedance tuning rule for robot:

$$\begin{aligned} \hat{D}_h + D_d &= \bar{D} \\ \hat{K}_h + K_d &= \bar{K}, \end{aligned} \tag{5}$$

where $\bar{D}, \bar{K} \in \mathbb{R}^{n\times n}$ are given positive diagonal matrices, $\hat{D}_h$ and $\hat{K}_h$ are the estimated matrices of D_h and K_h, respectively. According to the proposed tuning rule (5), robot can adjust its desired impedance parameters to adapt to different humans' impedance. Therefore, we will propose an identification method to obtain the human impedance parameters.

For ensuring the operational safety, robot should follow human in a limited area and with a constrained speed. To address this issue, we will propose full-state constraints (i.e., position constraints and velocity constraints) in trajectory tracking in the Cartesian space, i.e., for $\forall t > 0$, $|x_i(t)| \leq k_{1i}$, $|\dot{x}_i(t)| \leq k_{2i}$. k_1 and k_2 denote predefined constrained constant vectors and $i = 1, 2, ..., n$.

Indicated by Fig. 2, four parts are considered in the controller design. First, in order to decrease the interaction force f, we propose a method to obtain the estimated value $\hat{x}_d$ of human motion intention. Second, in the inner trajectory tracking control loop, if x tracks the virtual desired trajectory x_r which is acquired by the output of the outer loop, the robot would track the target impedance model, and NNs are utilized to address uncertainties in dynamic model of robot. Third, we propose an impedance learning method to acquire the human arm impedance and design a tuning rule to adjust desired impedance parameters of robot for efficient collaboration. Eventually, full-state constraints are considered in the trajectory tracking control to ensure safety of human-robot interaction.

III. Control Design

A. Human Motion Intention Estimation

Suppose that D_h and K_h are unknown functions of system state variables, we cannot obtain $\hat{x}_d$ by (2) directly. We employ the method in [14] to estimate x_d according to x, $\dot{x}$ and f as follows:

$$\hat{x}_d = Y(f, x, \dot{x}). \tag{6}$$

$Y(\cdot)$ is an unknown function and may be nonlinear, so an effective estimation method should be used to approximate $Y(\cdot)$. As an important online learning NN method, RBFNN can be used to estimate x_d and

an adaptive method is proposed to estimate the actual weights of RBFNN. A typical RBFNN structure is described as follows

$$\hat{x}_{di} = \hat{\Theta}_i^T S_i(\eta_i) + \varepsilon_i, \tag{7}$$

where the input of RBFNN is η_i=[f_i^T, x_i^T, $\dot{x}_i^T$], $S_i(\cdot)$ is the radial basis function, $\hat{\Theta}_i$ and ε_i denote the estimated weight and the estimation error, respectively. According to (2), interaction force f will become small if x gets close to x_d. Therefore, $\hat{\Theta}_i$ is adjusted based on the steepest descent method with respect to the cost function

$$E_{Mi} = \frac{1}{2} f_i^2, \tag{8}$$

where f_i is the interaction force in one direction. Then we propose the adaptation law as follows

$$\begin{aligned} \dot{\hat{\Theta}}_i &= -\beta_i \frac{\partial E_{Mi}}{\partial \hat{\Theta}_i} \\ &= -\beta_i \frac{\partial E_{Mi}}{\partial f_i} \frac{\partial f_i}{\partial \hat{x}_{di}} \frac{\partial \hat{x}_{di}}{\partial \hat{\Theta}_i} \\ &= -\beta_i f_i K_{hi} S_i(\eta_i) \\ &= -\gamma_i f_i S_i(\eta_i), \end{aligned} \tag{9}$$

where β_i is a positive scalar, and β_i and K_{hi} are absorbed by γ_i (the detailed derivation seen in ***Appendix B***). So $\hat{\Theta}_i$ can be designed as

$$\hat{\Theta}_i = \hat{\Theta}_i(0) - \gamma_i \int_0^t [f_i(\omega) S(\eta_i(\omega))] d\omega. \tag{10}$$

Then human motion intention estimation $\hat{x}_d$ can be acquired based on (7) and (10).

B. Human Impedance Learning

If we obtain the estimates $\hat{D}_h$ and $\hat{K}_h$ in dynamic model of human (2), we can adjust impedance parameter matrices of robot in (4) based on the tuning rule (5) for robot adapting to different interactive situations. In this section, we propose a human impedance learning method for obtaining $\hat{D}_h$ and $\hat{K}_h$. If we have the estimates of D_h, K_h and x_d, the estimated interaction force $\hat{f}$ can be written as

$$\hat{f} = -\hat{D}_h \dot{x} + \hat{K} z, \tag{11}$$

where $z = x - \hat{x}_d$. As $\hat{x}_d$ can be obtained in Section 3.1, z and $\dot{x}$ are known in (11), and actual interaction force f is measurable, we apply parameter estimation method to obtain the unknown matrices. Least square (LS) method can be employed in system parameter estimation, based on which we consider a cost function

$$E_{Li} = \sum_{j=1}^{N} (f_{ij} - \hat{f}_{ij})^2, \tag{12}$$

where j denotes the sampling number. In particular, we want to make partial derivatives of E_{Li} with respect to D_h and K_h zero:

$$\frac{\partial E_{Li}}{\partial D_h} = 0, \frac{\partial E_{Li}}{\partial K_h} = 0. \tag{13}$$

In practical human-robot interactive processes, D_h and K_h can be time-varying. Based on the moving average algorithm, we can get the latest sampling region for improving the estimation accuracy of the time-varying parameters. We obtain the estimated parameters $\hat{D}_h(t)$ and $\hat{K}_h(t)$ as below

$$\begin{aligned}
\begin{bmatrix} \hat{D}_h(t) \\ \hat{K}_h(t) \end{bmatrix} &= \begin{bmatrix} -\sum_{j=1}^{S} \dot{x}_{ij}^2 & \sum_{j=1}^{S} \dot{x}_{ij} z_{ij} \\ -\sum_{j=1}^{S} z_{ij} \dot{x}_{ij} & \sum_{j=1}^{S} z_{ij}^2 \end{bmatrix}^{-1} \times \begin{bmatrix} \sum_{j=1}^{S} \dot{x}_{ij} f_{ij} \\ \sum_{j=1}^{S} z_{ij} f_{ij} \end{bmatrix} (s \leq S) \\
&= \begin{bmatrix} -\sum_{j=s-S+1}^{s} \dot{x}_{ij}^2 & \sum_{j=s-S+1}^{s} \dot{x}_{ij} z_{ij} \\ -\sum_{j=s-S+1}^{s} z_{ij} \dot{x}_{ij} & \sum_{j=s-S+1}^{s} z_{ij}^2 \end{bmatrix}^{-1} \times \begin{bmatrix} \sum_{j=s-S+1}^{s} \dot{x}_{ij} f_{ij} \\ \sum_{j=s-S+1}^{s} z_{ij} f_{ij} \end{bmatrix} (s > S),
\end{aligned} \tag{14}$$

where s denotes the sampling number at time t and S denotes the sampling interval in a sampling time period T. According to the proposed method, the estimation of time-varying $\hat{D}_h(t)$ and $\hat{K}_h(t)$ can be obtained (the detailed derivation seen in ***Appendix B***). To ensure symmetric positive definiteness (SPD) for $\hat{D}_h$ and $\hat{K}_h$, we adopt the method in [53] to compute $\hat{D}'_h$ and $\hat{K}'_h$ as the SPD matrices nearest to $\hat{D}_h$ and $\hat{K}_h$ according to the Frobenius norm as follows:

$$\begin{aligned}
\hat{D}'_h &= \frac{A+P}{2}, A = \frac{\hat{D}_h + \hat{D}_h^T}{2}, \\
\hat{K}'_h &= \frac{B+Y}{2}, B = \frac{\hat{K}_h + \hat{K}_h^T}{2}.
\end{aligned} \tag{15}$$

where P and Y denote the symmetric polar factor which can be found from the singular value decomposition of A and B, respectively, with $A = LP$, $B = RY$, $L^T L = I$, $R^T R = I$. Therefore, we can obtain desired impedance parameter matrices of robot D_d and K_d according to the tuning rule (5).

C. Tracking Control with Full-state Constraints

In previous sections, D_d, K_d and $\hat{x}_d$ are obtained, so we can calculate virtual desired reference trajectory x_r according to (3). If x tracks x_r, the robot would track the target impedance model. For ensuring the operational safety, the robot should follow the human arm in a constrained area and with a constrained speed. BLF-based method is used in tracking control for avoiding constraint violation. In the first part of this section, a model-based control is developed considering position and velocity constraints.

I. Model-based (MB) Control

Suppose that the dynamic model of robot is known for the designer, i.e., $M_t(x)$, $C_t(x,\dot{x})$ and $G_t(x)$ are known. For convenience of analysis, denoting $x_1 = x$, $x_2 = \dot{x}$, the dynamic model of robot in state-space form is described as follows:

$$\begin{aligned} \dot{x}_1 &= x_2 \\ \dot{x}_2 &= M_t(x_1)^{-1}(u - f - C_t(x_1,x_2)x_2 - G_t(x_1)) \\ y &= x_1. \end{aligned} \tag{16}$$

Then we define the tracking error as

$$e_1 = x_1 - x_r, e_2 = x_2 - \alpha_1, \tag{17}$$

where α_1 denotes a virtual stabilization variable to be defined later. Choose a log-type BLF candidate V_1 as follows:

$$V_1 = \frac{1}{2}\sum_{i=1}^{n} \ln \frac{k_{ai}^2}{k_{ai}^2 - e_{1i}^2}, \tag{18}$$

where k_a and k_b denote tracking error constraints, where $k_a = k_1 - \bar{k}_1$, $k_b = k_2 - \bar{k}_2$, $k_a = [k_{a1}, k_{a2}, ..., k_{an}]$, $k_b = [k_{b1}, k_{b2}, ..., k_{bn}]$. $\bar{k}_1$ and $\bar{k}_2$ denote vectors composed of the maximum absolute values of x_{ri} and α_{1i}, respectively. They can be described as $x_{ri} \leq \bar{k}_{1i}$, $\alpha_{1i} \leq \bar{k}_{2i}$. Differentiating V_1 with respect to time, we obtain

$$\dot{V}_1 = \sum_{i=1}^{n} \frac{e_{1i}\dot{e}_{1i}}{k_{ai}^2 - e_{1i}^2}. \tag{19}$$

Then differentiating e_1 with respect to time, we obtain

$$\dot{e}_1 = e_2 + \alpha_1 - \dot{x}_r. \tag{20}$$

We define α_1 in (17) as follows:

$$\alpha_1 = \dot{x}_r - A, \tag{21}$$

where

$$A = \begin{bmatrix} (k_{a1}^2 - e_{11}^2) g_{11} e_{11} \\ (k_{a2}^2 - e_{12}^2) g_{12} e_{12} \\ \cdots \\ (k_{an}^2 - e_{1n}^2) g_{1n} e_{1n} \end{bmatrix}, \tag{22}$$

where g_{1i} is gain parameter. Substituting (20), (21) and (22) into (19), we have

$$\dot{V}_1 = -\sum_{i=1}^{n} g_{1i} e_{1i}^2 + \sum_{i=1}^{n} \frac{e_{1i} e_{2i}}{k_{ai}^2 - e_{1i}^2}. \tag{23}$$

Then we construct a BLF candidate V_2 as follows:

$$V_2 = V_1 + \frac{1}{2} e_2^T M_t(x_1) e_2 + \frac{1}{2} \sum_{i=1}^{n} \ln \frac{k_{bi}^2}{k_{bi}^2 - e_{2i}^2}. \tag{24}$$

Then differentiating V_2 with respect to time, we obtain

$$\begin{aligned} \dot{V}_2 &= -\sum_{i=1}^{n} g_{1i} e_{1i}^2 + \sum_{i=1}^{n} \frac{e_{1i} e_{2i}}{k_{ai}^2 - e_{1i}^2} + \sum_{i=1}^{n} \frac{e_{2i} \dot{e}_{2i}}{k_{bi}^2 - e_{2i}^2} \\ &\quad + e_2^T [u_m - f - C_t(x_1, x_2)\alpha_1 - G_t(x_1) - M_t(x_1)\dot{\alpha}_1]. \end{aligned} \tag{25}$$

Differentiating e_2 with respect to time, we can obtain

$$\begin{aligned} \dot{e}_2 &= \dot{x}_2 - \dot{\alpha}_1 \\ &= M_t(x_1)^{-1} (u_m - f - C_t(x_1, x_2) x_2 - G_t(x_1)) - \dot{\alpha}_1. \end{aligned} \tag{26}$$

Substituting (26) to (25), we can design the MB control input as follows:

$$\begin{aligned} u_m &= -G_2 e_2 + C_t(x_1, x_2)\alpha_1 + G_t(x_1) + M_t(x_1)\dot{\alpha}_1 + f \\ &\quad - (e_2^T)^+ \sum_{i=1}^{n} \frac{e_{1i} e_{2i}}{k_{ai}^2 - e_{1i}^2} - (e_2^T)^+ \sum_{i=1}^{n} \frac{e_{2i}(a_i - \dot{\alpha}_{1i})}{k_{bi}^2 - e_{2i}^2} \end{aligned} \tag{27}$$

where $(e_2^T)^+$ denotes the Moore-Penrose inverse of e_2^T, G_2 denotes gain matrix. We can obtain the following relationship according to the property of Moore-Penrose inverse:

$$e_2^T(e_2^T)^+ = \begin{cases} 0, & e_2 = [0,0,...,0]^T \\ 1, & \text{otherwise.} \end{cases} \tag{28}$$

Under the control input u_m in (27), $\dot{V}_2$ satisfies the following condition:

$$\dot{V}_2 = -\sum_{i=1}^{n} k_{1i} e_{1i}^2 - e_2^T G_2 e_2 < 0. \tag{29}$$

So we can conclude that tracking errors e_1 and e_2 remain in the interval $\forall t > 0, -k_{ai} \leq e_{1i} \leq k_{ai}, -k_{bi} \leq e_{2i} \leq k_{bi}$, and the states x_1 and x_2 remain in the interval $\forall t > 0, |x_{1i}(t)| \leq k_{1i}, |\dot{x}_{2i}(t)| \leq k_{2i}$.

Remark 2: We consider a special situation when $e_2 = \mathbf{0}$, which leads to $\dot{V}_2 = -\sum_{i=1}^{n} k_{1i} e_{1i}^2 \leq 0$ in (29). The asymptotic stability of the system can be drawn by the Barbalat lemma. In this paper, we consider $e_2 \neq \mathbf{0}$ and design controllers (27) and (32).

II. Adaptive RBFNN Control with Full-state Feedback

To address uncertainties in the dynamic model of robot, i.e., $M_t(x)$, $C_t(x,\dot{x})$ and $G_t(x)$ are unknown, an adaptive NN control design is proposed. We design NN adaptive law as follows:

$$\dot{\hat{W}}_i = -\Gamma_i [S_i(Z_i) e_{2i} + \sigma_i \hat{W}_i], i = 1,2,...,n \tag{30}$$

where $\Gamma_i = \Gamma_i^T$ denotes positive gain matrix, $\hat{W}_i$ denotes the weight estimate of NN and σ_i is a small positive constant for improving system robustness. The input of NN is Z_i=[x_1^T, x_2^T, α^T, $\dot{\alpha}^T$], and $\hat{W}^T S(Z)$ is utilized to estimate $W^{*T} S(Z)$:

$$W^{*T} S(Z) = C_t(x_1, x_2)\alpha_1 + G_t(x_1) + \dot{\alpha}_1 M_t(x_1) - \varepsilon(Z), \tag{31}$$

where W_i^* denotes actual NN weight, $\varepsilon(Z)$ denotes estimation error which is in bounds over the compact set Ω, $\forall Z \in \Omega$, $||\varepsilon(Z)|| < \bar{\varepsilon} (\bar{\varepsilon} > 0)$. We design NN control input u as follows:

$$\begin{aligned} u = &-G_3 e_2 + \hat{W}^T S(Z) + f - (e_2^T)^+ \sum_{i=1}^{n} \frac{e_{1i} e_{2i}}{k_{ai}^2 - e_{1i}^2} \\ &- (e_2^T)^+ \sum_{i=1}^{n} \frac{e_{2i}(a_i - \dot{\alpha}_{1i})}{k_{bi}^2 - e_{2i}^2} - (e_2^T)^+ \sum_{i=1}^{n} \frac{g_{1i} e_{1i}^2}{k_{ai}^2 - e_{1i}^2} - (e_2^T)^+ \sum_{i=1}^{n} \frac{g_{2i} e_{2i}^2}{k_{bi}^2 - e_{2i}^2}, \end{aligned} \tag{32}$$

where g_{2i} and G_3 denote the gain parameter and positive definite gain matrix, respectively. Then we construct another BLF functions V_3 as

$$V_3 = V_2 + \frac{1}{2}\sum_{i=1}^{n} \tilde{W}_i^T \Gamma_i^{-1} \tilde{W}_i, \tag{33}$$

where the weight error $\tilde{W}_i = W_i^* - \hat{W}_i$. Then we differentiate V_3 as

$$\begin{aligned}\dot{V}_3 = &-\sum_{i=1}^{n} g_{1i} e_{1i}^2 + \sum_{i=1}^{n} \frac{e_{1i} e_{2i}}{k_{ai}^2 - e_{1i}^2} + \sum_{i=1}^{n} \frac{e_{2i}\dot{e}_{2i}}{k_{bi}^2 - e_{2i}^2} \\ &+ e_2^T [u - f(t) - C_t(x_1, x_2)\alpha_1 - G_t(x_1) - M_t(x_1)\dot{\alpha}_1].\end{aligned} \tag{34}$$

We have

$$\begin{aligned}\dot{V}_3 \leq &-\sum_{i=1}^{n} g_{1i} e_{1i}^2 - e_2^T G_2 e_2 - \sum_{i=1}^{n} \frac{g_{1i} e_{1i}^2}{k_{ai}^2 - e_{1i}^2} - e_2^T \varepsilon(Z) \\ &- \sum_{i=1}^{n} \frac{g_{2i} e_{2i}^2}{k_{bi}^2 - e_{2i}^2} + e_2^T \hat{W}^T S(Z) - e_2^T W^{*T} S(Z) \\ &+ \sum_{i=1}^{n} \tilde{W}_i^T \Gamma_i^{-1} \{-\Gamma_i [S_i(Z) e_{2,i} + \sigma_i \hat{W}_i]\} \\ &\leq -e_2^T (G_2 - I) e_2 - \sum_{i=1}^{n} \frac{g_{1i} e_{1i}^2}{k_{ai}^2 - e_{1i}^2} - \sum_{i=1}^{n} \frac{g_{2i} e_{2i}^2}{k_{bi}^2 - e_{2i}^2} \\ &+ \frac{1}{2}||\varepsilon(Z)||^2 + \frac{\sigma_i}{2}(||W_i^*||^2 - ||\tilde{W}_i||^2) \\ &\leq -\rho V_3 + C,\end{aligned} \tag{35}$$

where

$$\begin{aligned}\rho &= \min(\min(2g_{1i}), \min(2g_{2i}), \frac{2\lambda_{\min}(G_2 - I)}{\lambda_{\max}(M_t(x))}, \min(\frac{\sigma_i}{\Gamma_i^{-1}})) \\ C &= \frac{1}{2}||\bar{\varepsilon}||^2 + \frac{\sigma_i}{2}||W_i^*||^2.\end{aligned} \tag{36}$$

where $\lambda_{\min}$ and $\lambda_{\max}$ denote the minimum and maximum eigenvalues of a matrix.

Theorem 1: For initial conditions $|x_{1i}(0)| \leq k_{1i}, |x_{2i}(0)| \leq k_{2i}$, control law (32) ensures that all error signals are semi-globally uniformly bounded (SGUB) and position and velocity constraints are not violated, i.e., $\forall t > 0$, $|x_{1i}(t)| \leq k_{1i}, |x_{2i}(t)| \leq k_{2i}$. The closed-loop error signals e_1, e_2 and $\tilde{W}$ remain in compact sets

Ω_{e_1}, Ω_{e_2}, $\Omega_{\tilde{W}}$, respectively:

$$\Omega_{e_1} = \{e_1 \varepsilon R^n | \ ||e_1|| \leq \sqrt{k_{ai}^2(1-e^{-Q})}, i = 1,2,3,...,n\}$$
$$\Omega_{e_2} = \{e_2 \varepsilon R^n | \ ||e_2|| \leq \sqrt{\frac{Q}{\lambda_{\min}(M_t(x))}}\} \cap$$
$$\{e_2 \varepsilon R^n | \ ||e_2|| \leq \sqrt{k_{bi}^2(1-e^{-Q})}, i = 1,2,3,...,n\}$$
$$\Omega_{\tilde{W}} = \{\tilde{W} \varepsilon R^{l \times n} | \ ||\tilde{W}|| \leq \sqrt{\frac{Q}{\lambda_{\min}(\Gamma^{-1})}}\}, \tag{37}$$

where $Q = V_3(0) + C/\rho$ with positive constants C and ρ given in (36).

IV. Simulation

In simulations, two-link revolute joint robot shown in Fig. 1(a) is in interaction with human, and interaction force generated by human is applied on the handle near the end-effector of robot.

A. Simulation Results about Human Impedance Learning

In this part, we consider unknown fixed and time-varying human impedance in two cases, and parameter matrices $\bar{D}$ and $\bar{K}$ in impedance tuning rule (5) are designed as $\bar{D} = \text{diag}[3,3]$ and $\bar{K} = \text{diag}[3,3]$. We consider fixed impedance $D_h = \text{diag}[1,1]$, $K_h = \text{diag}[2,2]$ in the first case, and time-varying impedance $D_h = \text{diag}[1+0.2\sin(t), 1+0.2\sin(t)]$ in the second case. We utilize least square method (LS) combined with moving average algorithm in (14) to obtain estimated impedance matrices $\hat{D}_h$ and $\hat{K}_h$, and SPD can be ensured based on (15). (5) is employed to tune the robot's desired impedance online based on estimated impedance. In Fig. 3(a) and Fig. 3(b), we can find that fixed or time-varying damper parameters of human can be estimated and we can obtain desired damper parameters of robot. In a similar way, stiffness parameters by our proposed method can be obtained.

B. Simulation Results about Human Intention Estimation

We employ our proposed RBFNN method to estimate the human motion intention x_d in (7). Adaptation law (9) is designed to adjust $\hat{\Theta}_i$ in (10). Human motion intention estimation is calculated based on (7). We choose RBFNN centers in the region of $[-1,1]$, number of nodes in the RBFNN as 2^6, and we define the initial value of the RBFNN weights Θ_i as 0. Indicated from Fig. 4(a), we set different initial human motion intention $x_{d1}(0)$ as 1.10m, 1.65m and 1.80m, respectively. Under our human motion intention

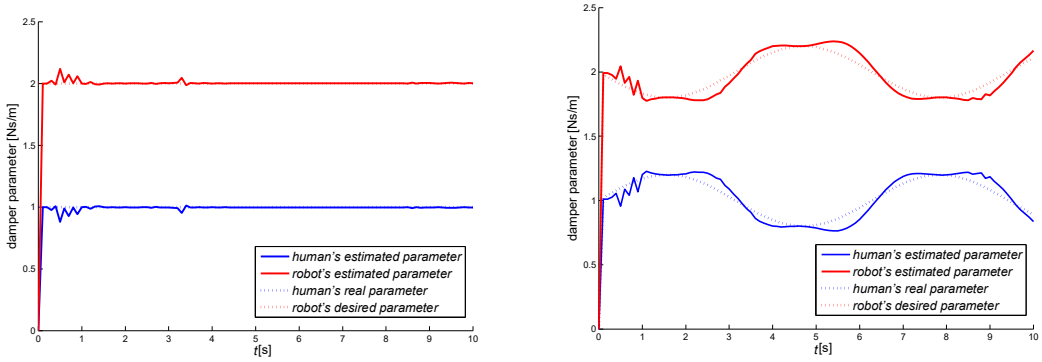

(a) fixed human impedance. (b) time-varying human impedance.

Fig. 3: IV. A-human impedance learning.

estimation method, interaction forces are all below 2N in pHRI. Fig. 4(b) shows that errors between x_{d1} and $\hat{x}_{d1}$ in three different conditions all converge to zero, where x_{d1} and $\hat{x}_{d1}$ denote human motion intention and its estimate in the x-axis in the task space, respectively.

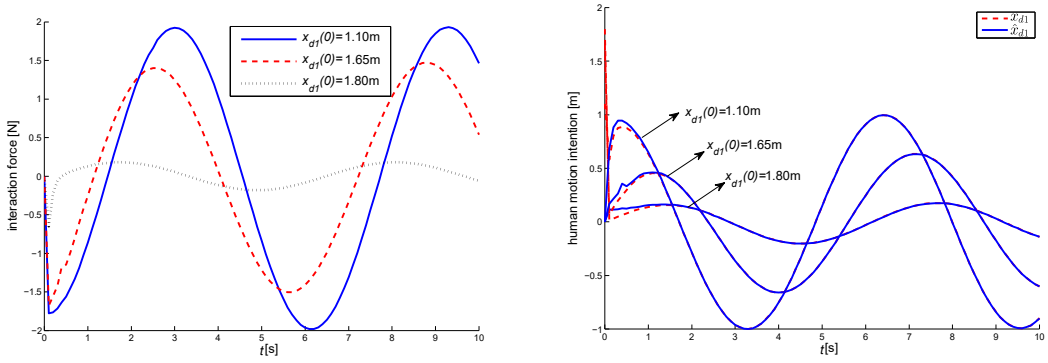

(a) interaction force. (b) human motion intention estimation.

Fig. 4: IV. B-human interaction force and motion intention estimation.

C. Simulation Results about Tracking Control and Full-state Constraints

In this part, we evaluate our proposed method compared with the situation without constraints in controller design. For design of our proposed method with constraints in (32), the tracking error constraints are set as $k_{a1} = 0.4\text{m}$, $k_{a2} = 0.4\text{m}$, $k_{b1} = 0.4\text{m/s}$, $k_{b2} = 0.4\text{m/s}$ and full-state constraint vectors $k_1 = [1.5\text{m}; 1.5\text{m}]$,

$k_2 = [1.5\text{m/s}; 1.5\text{m/s}]$; gain parameters in (32) $g_{11} = 2$, $g_{12} = 2$, $g_{21} = 10$, $g_{22} = 10$, $G_3 = \text{diag}[10, 10]$. Fig. 5(a) and Fig. 5(b) illustrate the comparative position tracking results. Fig. 5(c) and Fig. 5(d) illustrate the comparative velocity tracking results. Indicated from Fig. 5, under our proposed controller all error signals do not transgress constraints, and tracking errors converge to a small region around zero when initial states are in bounds. Compared with control design with no constraints, tracking errors with constraints are smaller. Indicated from Fig. 5(c), the velocity tracking error in x-axis is over bound obviously without constraints.

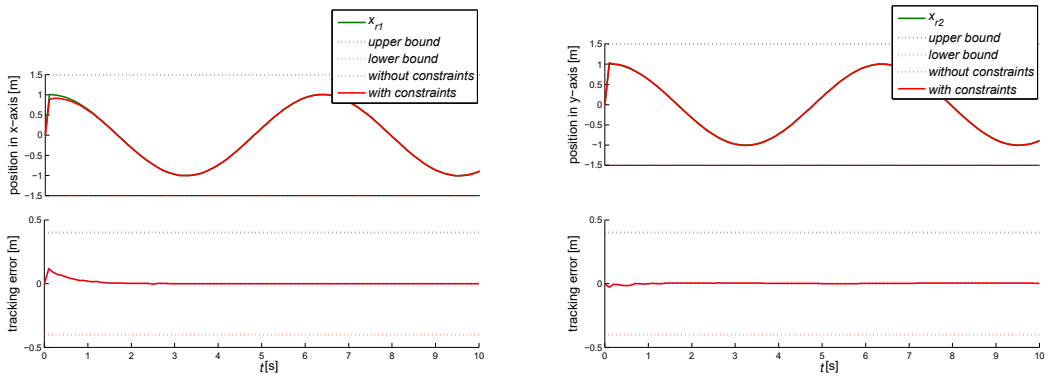

(a) position in x-axis.

(b) position in y-axis.

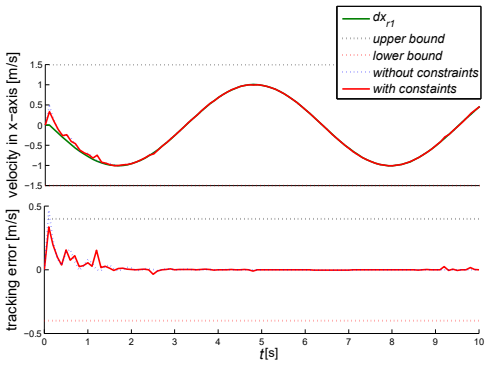

(c) velocity in x-axis.

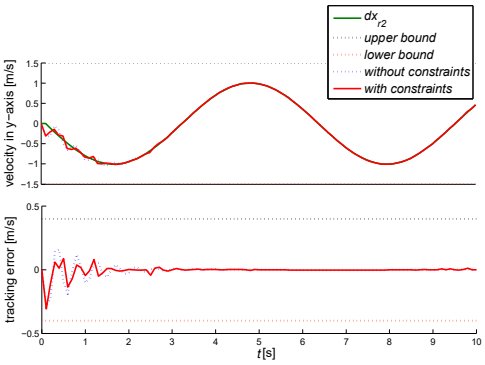

(d) velocity in y-axis.

Fig. 5: IV. C-tracking performance with and without constraints.

D. Synthetic Simulation

In this part, both human impedance learning and motion intention estimation in pHRI subject to constraints are considered, which are set the same as above. The robot's initial position $x_1(0)$=[0.85m, 1.05m], initial

velocity $x_2(0)$=[0m/s, 0m/s], and we set the robot's virtual reference trajectory x_r as

$$x_r = \begin{bmatrix} (0.1\sin(t)+\cos(t))\text{m} \\ (0.1\sin(t)+\cos(t))\text{m} \end{bmatrix}. \tag{38}$$

For our proposed RBFNN control, we choose gain parameters as $g_{11}=2$, $g_{12}=2$, $g_{21}=5$, $g_{22}=5$, $K_3=\text{diag}[10,10]$, RBFNN centers in the region of $[-1,1]$, the initial value of the RBFNN weight as 0, the number of nodes in the RBFNN as 2^8. Γ_1 and Γ_2 are chosen as 100 and σ_i is chosen as 0.002. Fig. 6(a)

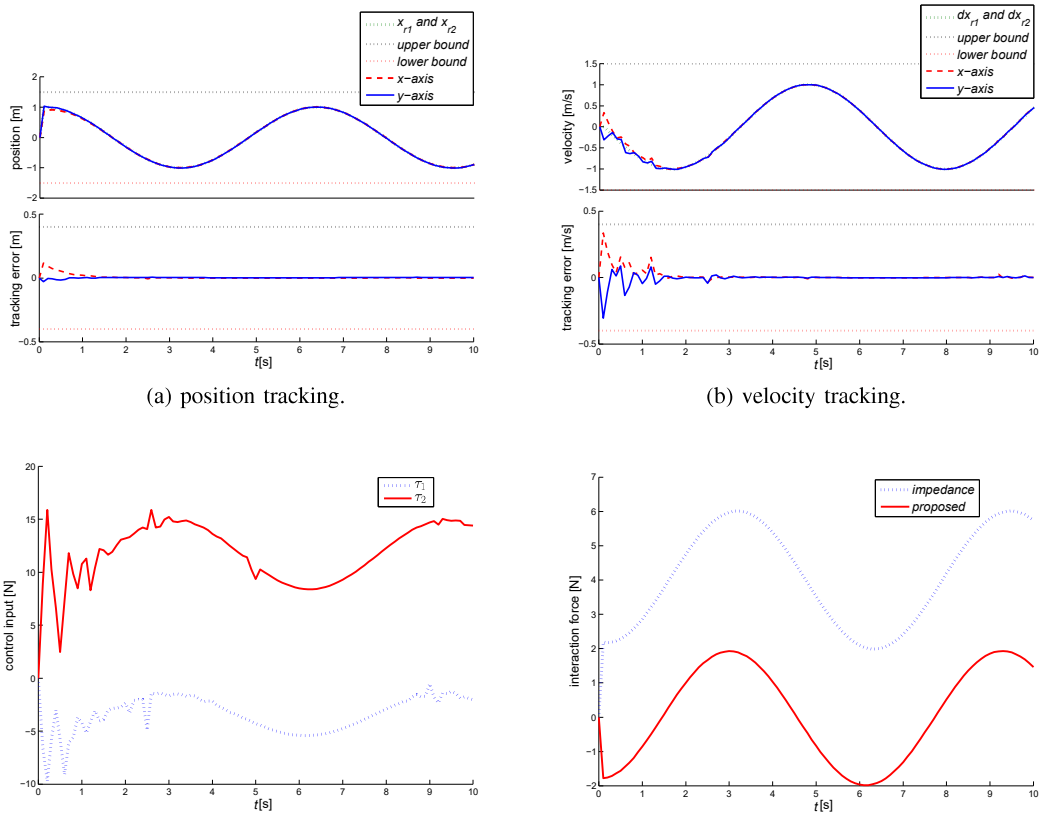

(a) position tracking.

(b) velocity tracking.

(c) control input.

(d) interaction force.

Fig. 6: IV. D-tracking performance, control input and interaction force.

and Fig. 6(b) show that control (32) can guarantee that tracking errors converge to a small region around zero, and all error signals do not violate error constraints. In Fig. 6(c), we can see that corresponding control inputs are bounded. Indicated by Fig. 6(d), the interaction force under the traditional control design not considering motion intention estimation is larger than the force under the proposed control design considering the human motion intention estimation.

V. Experiment

A. Experiment Setup

As shown in Fig. 7, Baxter robot is used in our experiment. Each arm of the Baxter bimanual robot has 7 flexible joints, i.e., joints S_0, S_1, E_0, E_1, W_0, W_1 and W_2, and each joint has angle and torque sensors. The resolution of angle sensors is 0.022 degree per tick, and the maximum torques are 50N/m in joints (S_0, S_1, E_0, E_1) and 15N/m in joints (W_0, W_1, W_2). Due to the limited computing speed of computers, two computers (Computer 1 and Computer 2) are employed for controlling the Baxter robot and calculation in this experiment. Computer 2 is employed to calculate the dynamics compensation by RBFNN in MATLAB SIMULINK and transfer the results to Computer 1 by Ethernet. Computer 1 is utilized to receive the angle, angular velocity and torque information from the Baxter robot and generate control signals to control the robot by Robot Operating System SDK (RSDK) in Ubuntu 14.04 LTS. Robot operating system (ROS) is a robot development framework that is used for integrating software libraries and tools for building robot applications.

We design an experiment where a human subject (age: 24; height: 172cm; weight: 61kg) collaborates with the right arm of Baxter robot to perform an object co-transporting task. Indicated from Fig. 1(b), the task objective is to move "orange" on the table to "cup" by human's and robot's collective efforts. Gripper of the robot is controlled to grasp or release the "orange" by a button near the gripper operated by human subject manually. Human subject knows the position of target "cup" through vision, and he guides the robot arm by physical interaction to grasp "orange" from the table, move towards "cup" and release it to "cup". The snapshot of experiment is shown in Fig. 1(b). For our proposed RBFNN control in (32), the number of nodes in the RBFNN is set as 7^3 for each $\phi_i(Z)$, and variance of centers is set as $\eta = 0.75$. Γ_i in adaptation law is set as $500I$ and $\sigma_i = 0.02$. The control gain matrices G_3=diag$[17.70, 15.00, 15.70, 10.02, 10.30, 14.60, 22.00]$, and $g_{11} = 7.10, g_{12} = 22.00, g_{13} = 2.00, g_{14} = 2.75, g_{15} = 4.10, g_{16} = 4.10, g_{17} = 5.6,\ g_{21} = 5.1, g_{22} = 12.00, g_{23} = 1.20, g_{24} = 2.50, g_{25} = 2.10, g_{26} = 2.10, g_{27} = 4.50$.

B. Case 1: Comparative Experiments about Motion Intention Estimation

In this case, we compare our method with human motion intention estimation with the method without estimation. We employ our proposed RBFNN method to estimate human motion intention x_d in (7).

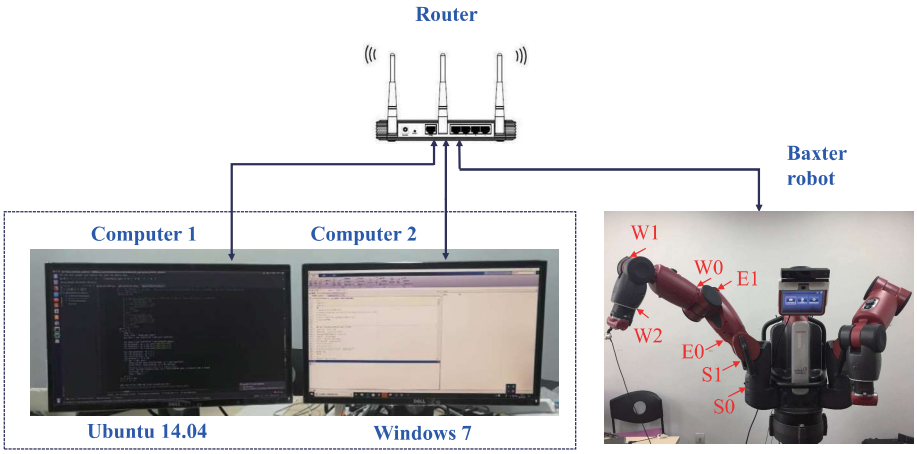

Fig. 7: Illustration of the experiment setup.

Adaptation law (9) is designed to adjust $\hat{\Theta}_i$ in (10). Human motion intention estimation is calculated based on (7). We choose RBFNN centers in the region of $[-1, 1]$, nodes number in RBFNN as 2^6, and we define the initial value of the RBFNN weights Θ_i as 0. Methods with and without human motion intention estimation are compared in the same task process shown in Fig. 1(b), which shows that they track an almost same trajectory from the same initial position to the same target position in about 20s. Interaction torques can be measured by toque sensors in robot internal platform. Seen from Fig. 8(a) and Fig. 8(b), we can find that interaction torques with human motion intention estimation are much smaller than those without estimation in some joints, such as joints S_0 (in 5s-14s), S_1 (in 15s-20s), E_0 (10s-13s), E_1 (15s-22s), W_0 (10s-12s), W_1 (15s-20s), and interaction torques without human motion intention estimation are larger than those with human motion intention estimation. Therefore, we can conclude that human makes more effort in the task when human intention estimation is not involved. We notice that torques in W_2 are almost zero in Fig. 8(a) and Fig. 8(b) because human subject may not use the joint in the task. The comparative results show that the robot can collaborate with human subject to perform tasks more actively using our proposed method.

C. Case 2: Comparative Experiments about Constraints

In this case, the same task is performed, with gain and NN parameters set the same as those in Case 1. The lower and upper bounds of joint errors are set as -0.10rad and 0.10rad in all joints in this case. We compare our proposed method with methods without constraints and the tracking errors are shown in Fig. 9. Indicated from Fig. 9, we find that all tracking errors under our proposed method are within

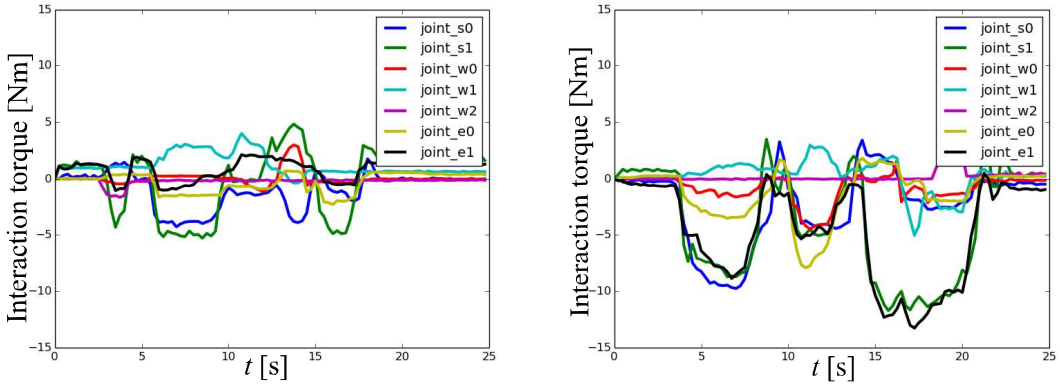

(a) with human motion intention estimation.

(b) without human motion intention estimation.

Fig. 8: Interaction torque in each joint of Baxter robot.

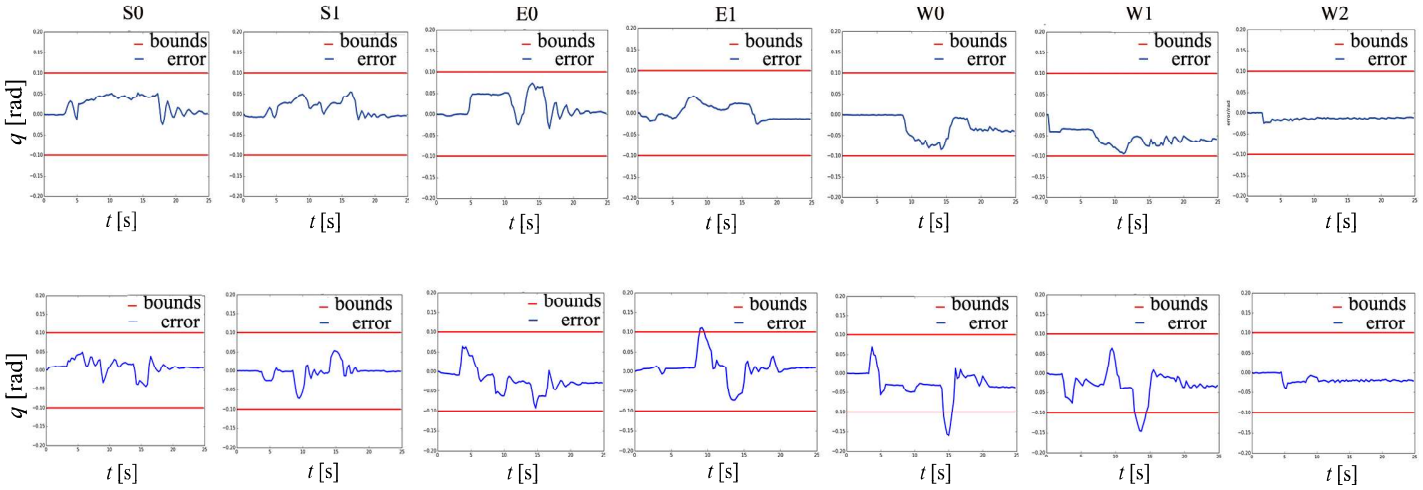

Fig. 9: Tracking performance with (top) and without (bottom) constraints.

the bounds $[-0.10\text{rad}, 0.10\text{rad}]$, but errors in some joints are over bounds under the method without constraints. With these results, we can conclude that our proposed method can ensure safe interaction in the task.

VI. Conclusion and Future Works

In this paper, we proposed an adaptive NN impedance control involving full-state constraints in human robot collaborative tasks. Estimation of human impedance and motion intention were considered to improve pHRI. Safe and compliant PHRI was ensured under our proposed method. RBFNNs were employed to estimate motion intention, and least square method was utilized in human impedance learning. RBFNNs were also employed in compensating for uncertainties in robot dynamics, while BLF was chosen to ensure position and velocity constraints not violated. Simulation and experiment results were presented to verify the effectiveness of our proposed method.

The current motion intention estimation method only allows a robot to follow the human partner, which is inapplicable to situations where the robot's autonomy is essential. This will be investigated in our future works. Impedance learning was tested in the experiments, where uncertainties due to human's involvement may lead to problems that need to be addressed. Finally, while a simplistic scenario was studied in this paper for proof of concept, in our future works, we will focus on specific collaborative tasks such as sawing and assembly.

VII. Acknowledgement

The authors would like to thank the Editor-in-Chief, the Associate Editor, and the anonymous reviewers for their constructive comments which helped to improve the quality and presentation of this paper. This work was supported by the National Natural Science Foundation of China under Grant 61873297, the China Postdoctoral Science Foundation under Grant 2018M630074 and the Fundamental Research Funds for the Central Universities under grant No. FRF-GF-18-027B.

References

[1] Wei He, Zhijun Li, and CL Philip Chen. A survey of human-centered intelligent robots: issues and challenges. *IEEE/CAA Journal of Automatica Sinica*, 4(4):602–609, 2017.

[2] José Ramón Medina, Martin Lawitzky, Alexander Mörtl, Dongheui Lee, and Sandra Hirche. An experience-driven robotic assistant acquiring human knowledge to improve haptic cooperation. In *Intelligent Robots and Systems (IROS), 2011 IEEE/RSJ International Conference on*, pages 2416–2422. IEEE, 2011.

[3] Chenguang Yang, Kunxia Huang, Hong Cheng, Yanan Li, and Chun-Yi Su. Haptic identification by ELM-controlled uncertain manipulator. *IEEE Transactions on Systems, Man, and Cybernetics: Systems*, 47(8):2398–2409, 2017.

[4] Jae H Chung. Control of an operator-assisted mobile robotic system. *Robotica*, 20(4):439–446, 2002.

[5] Keith Dupree, Chien-Hao Liang, Guoqiang Hu, and Warren E Dixon. Adaptive lyapunov-based control of a robot and mass–spring system undergoing an impact collision. *IEEE Transactions on Systems, Man, and Cybernetics, Part B (Cybernetics)*, 38(4):1050–1061, 2008.

[6] Marc H Raibert and John J Craig. Hybrid position/force control of manipulators. *Journal of Dynamic Systems, Measurement, and Control*, 102(127):126–133, 1981.

[7] Neville Hogan. Impedance control: An approach to manipulation. *Journal of Dynamic Systems, Measurement, and Control*, 107(1):8–16, 1985.

[8] Jaydeep Roy and Louis L Whitcomb. Adaptive force control of position/velocity controlled robots: theory and experiment. *IEEE Transactions on Robotics and Automation*, 18(2):121–137, 2002.

[9] Brecht Corteville, Erwin Aertbeliën, Herman Bruyninckx, Joris De Schutter, and Hendrik Van Brussel. Human-inspired robot assistant for fast point-to-point movements. In *Robotics and Automation, 2007 IEEE International Conference on*, pages 3639–3644, 2007.

[10] M. S. Erden and T. Tomiyama. Human-intent detection and physically interactive control of a robot without force sensors. *IEEE Transactions on Robotics*, 26(2):370–382, 2010.

[11] Jian Huang, Weiguang Huo, Wenxia Xu, Samer Mohammed, and Yacine Amirat. Control of upper-limb power-assist exoskeleton using a human-robot interface based on motion intention recognition. *IEEE Transactions on Automation Science and Engineering*, 12(4):1257–1270, 2015.

[12] Kohei Wakita, Jian Huang, Pei Di, Kosuke Sekiyama, and Toshio Fukuda. Human-walking-intention-based motion control of an omnidirectional-type cane robot. *IEEE/ASME Transactions On Mechatronics*, 18(1):285–296, 2013.

[13] Luka Peternel, Nikos Tsagarakis, and Arash Ajoudani. Towards multi-modal intention interfaces for human-robot co-manipulation. In *Intelligent Robots and Systems (IROS), 2016 IEEE/RSJ International Conference on*, pages 2663–2669. IEEE, 2016.

[14] Yanan Li and Shuzhi Sam Ge. Human–robot collaboration based on motion intention estimation. *IEEE/ASME Transactions on Mechatronics*, 19(3):1007–1014, 2014.

[15] Zhijun Li, Bo Huang, Arash Ajoudani, Chenguang Yang, Chun-Yi Su, and Antonio Bicchi. Asymmetric bimanual control of dual-arm exoskeletons for human-cooperative manipulations. *IEEE Transactions on Robotics*, 34(1):264–271, 2018.

[16] Chenguang Yang, Chao Zeng, Peidong Liang, Zhijun Li, Ruifeng Li, and Chun-Yi Su. Interface design of a physical human-robot interaction system for human impedance adaptive skill transfer. *IEEE Transactions on Automation Science and Engineering*, 15(1):329–340, 2018.

[17] Yanan Li and Shuzhi Sam Ge. Impedance learning for robots interacting with unknown environments. *IEEE Transactions on Control Systems Technology*, 22(4):1422–1432, 2014.

[18] Zhijun Li, Ting Zhao, Fei Chen, Yingbai Hu, Chun-Yi Su, and Toshio Fukuda. Reinforcement learning of manipulation and grasping using dynamical movement primitives for a humanoidlike mobile manipulator. *IEEE/ASME Transactions on Mechatronics*, 23(1):121–131, 2018.

[19] Byungchan Kim, Jooyoung Park, Shinsuk Park, and Sungchul Kang. Impedance learning for robotic contact tasks using natural actor-critic algorithm. *IEEE Transactions on Systems, Man, and Cybernetics, Part B (Cybernetics)*, 40(2):433–443, 2010.

[20] Toshio Tsuji, Koji Ito, and Pietro G Morasso. Neural network learning of robot arm impedance in operational space. *IEEE Transactions on Systems, Man, and Cybernetics, Part B (Cybernetics)*, 26(2):290–298, 1996.

[21] Pyung Hun Chang, Kyungbin Park, Sang Hoon Kang, Hermano Igo Krebs, and Neville Hogan. Stochastic estimation of human arm impedance using robots with nonlinear frictions: An experimental validation. *IEEE/ASME Transactions on Mechatronics*, 18(2):775–786, 2013.

[22] Leonel Rozo, Sylvain Calinon, Darwin Caldwell, Pablo Jimenez, and Carme Torras. Learning collaborative impedance-based robot behaviors. In *Twenty-Seventh AAAI Conference on Artificial Intelligence*, pages 1422–1428, 2013.

[23] Guangyu Wu, Jian Sun, and Jie Chen. Optimal linear quadratic regulator of switched systems. *IEEE Transactions on Automatic Control*, 2018.

[24] Changyin Sun and Youshen Xia. An analysis of a neural dynamical approach to solving optimization problems. *IEEE Transactions on Automatic Control*, 54(8):1972–1977, 2009.

[25] Mou Chen and Gang Tao. Adaptive fault-tolerant control of uncertain nonlinear large-scale systems with unknown dead zone. *IEEE Transactions on Cybernetics*, 46(8):1851–1862, 2016.

[26] Wei He, Xiuyu He, Mingfo Zou, and Hongyi Li. PDE model-based boundary control design for a flexible robotic manipulator with input backlash. *IEEE Transactions on Control Systems Technology*, 27(2):790–797, 2019.

[27] Hongyi Li, Shiyi Zhao, Wei He, and Renquan Lu. Adaptive finite-time tracking control of full state constrained nonlinear systems with dead-zone. *Automatica*, 100:99–107, 2019.

[28] Changyin Sun, Wei He, and Jie Hong. Neural network control of a flexible robotic manipulator using the lumped spring-mass model. *IEEE Transactions on Systems, Man, and Cybernetics: Systems*, 47(8):1863–1874, 2016.

[29] Chenguang Yang, Yiming Jiang, Zhijun Li, Wei He, and Chun-Yi Su. Neural control of bimanual robots with guaranteed global stability and motion precision. *IEEE Transactions on Industrial Informatics*, 13(3):1162–1171, 2017.

[30] Chenguang Yang, Zhijun Li, Rongxin Cui, and Bugong Xu. Neural network-based motion control of an underactuated wheeled inverted pendulum model. *IEEE Transactions on Neural Networks and Learning Systems*, 25(11):2004–2016, 2014.

[31] Wei He, Tingting Meng, Xiuyu He, and Changyin Sun. Iterative learning control for a flapping wing micro aerial vehicle under distributed disturbances. *IEEE Transactions on Cybernetics*, 49(4):1524–1535, 2019.

[32] Rongxin Cui, Lepeng Chen, Chenguang Yang, and Mou Chen. Extended state observer-based integral sliding mode control for an underwater robot with unknown disturbances and uncertain nonlinearities. *IEEE Transactions on Industrial Electronics*, 64(8):6785–6795, 2017.

[33] Changyin Sun, Wei He, Weiliang Ge, and Cheng Chang. Adaptive neural network control of biped robots. *IEEE Transactions on Systems, Man, and Cybernetics: Systems*, 47(2):315–326, 2017.

[34] Changyin Sun, Hejia Gao, Wei He, and Yao Yu. Fuzzy neural network control of a flexible robotic manipulator using assumed mode method. *IEEE Transactions on Neural Networks and Learning Systems*, 29(11):5214–5227, 2018.

[35] Wei He and Shuzhi Sam Ge. Cooperative control of a nonuniform gantry crane with constrained tension. *Automatica*, 66:146–154, 2016.

[36] Shi-Lu Dai, Min Wang, and Cong Wang. Neural learning control of marine surface vessels with guaranteed transient tracking performance. *IEEE Transactions on Industrial Electronics*, 63(3):1717–1727, 2016.

[37] Hesheng Wang, Runxi Zhang, Weidong Chen, Xinwu Liang, and Rolf Pfeifer. Shape detection algorithm for soft manipulator based on fiber bragg gratings. *IEEE/ASME Transactions on Mechatronics*, 21(6):2977–2982, 2016.

[38] Rongxin Cui, Chenguang Yang, Yang Li, and Sanjay Sharma. Adaptive neural network control of auvs with control input

nonlinearities using reinforcement learning. *IEEE Transactions on Systems, Man, and Cybernetics: Systems*, 47(6):1019–1029, 2017.

[39] Mou Chen. Disturbance attenuation tracking control for wheeled mobile robots with skidding and slipping. *IEEE Transactions on Industrial Electronics*, 64(4):3359–3368, 2017.

[40] Zhijun Li, Bo Huang, Zhifeng Ye, Mingdi Deng, and Chenguang Yang. Physical human–robot interaction of a robotic exoskeleton by admittance control. *IEEE Transactions on Industrial Electronics*, 65(12):9614–9624, 2018.

[41] CL Philip Chen, Guo-Xing Wen, Yan-Jun Liu, and Zhi Liu. Observer-based adaptive backstepping consensus tracking control for high-order nonlinear semi-strict-feedback multiagent systems. *IEEE transactions on cybernetics*, 46(7):1591–1601, 2016.

[42] Zhengqiang Zhang and Shengyuan Xu. Observer design for uncertain nonlinear systems with unmodeled dynamics. *Automatica*, 51:80–84, 2015.

[43] Wei He and Yiting Dong. Adaptive fuzzy neural network control for a constrained robot using impedance learning. *IEEE Transactions on Neural Networks and Learning Systems*, 29(4):1174–1186, 2018.

[44] Wei He, Tingting Meng, Xiuyu He, and Shuzhi Sam Ge. Unified iterative learning control for flexible structures with input constraints. *Automatica*, 96:326–336, 2018.

[45] Wei He, Zhijun Li, Yiting Dong, and Ting Zhao. Design and adaptive control for an upper limb robotic exoskeleton in presence of input saturation. *IEEE Transactions on Neural Networks and Learning Systems*, 30(1):97–108, 2019.

[46] Zhijun Li, Ziting Chen, Jun Fu, and Changyin Sun. Direct adaptive controller for uncertain MIMO dynamic systems with time-varying delay and dead-zone inputs. *Automatica*, 63:287–291, 2016.

[47] Wei He, Yuhao Chen, and Zhao Yin. Adaptive neural network control of an uncertain robot with full-state constraints. *IEEE Transactions on Cybernetics*, 46(3):620–629, 2016.

[48] Keng Peng Tee, Shuzhi Sam Ge, and Eng Hock Tay. Barrier Lyapunov functions for the control of output-constrained nonlinear systems. *Automatica*, 45(4):918–927, 2009.

[49] Keng Peng Tee, Beibei Ren, and Shuzhi Sam Ge. Control of nonlinear systems with time-varying output constraints. *Automatica*, 47(11):2511–2516, 2011.

[50] Shuang Zhang, Yiting Dong, Yuncheng Ouyang, Zhao Yin, and Kaixiang Peng. Adaptive neural control for robotic manipulators with output constraints and uncertainties. *IEEE Transactions on Neural Networks and Learning Systems*, 29(11):5554–5564, 2018.

[51] Zhijun Li, Wang Yuan, Yao Chen, Fan Ke, Xiaoli Chu, and CL Philip Chen. Neural-dynamic optimization-based model predictive control for tracking and formation of nonholonomic multirobot systems. *IEEE Transactions on Neural Networks and Learning systems*, 29(12):6113–6122, 2018.

[52] Md Mozasser Rahman, Ryojun Ikeura, and Kazuki Mizutani. Investigation of the impedance characteristic of human arm for development of robots to cooperate with humans. *JSME International Journal Series C Mechanical Systems, Machine Elements and Manufacturing*, 45(2):510–518, 2002.

[53] Nicholas J Higham. Computing a nearest symmetric positive semidefinite matrix. *Linear algebra and its applications*, 103:103–118, 1988.

[54] Shuzhi Sam Ge, Chang Chieh Hang, and LC Woon. Adaptive neural network control of robot manipulators in task space. *IEEE Transactions on Industrial Electronics*, 44(6):746–752, 1997.

VIII. Appendix A

We consider an m degree-of-freedom (DOF) dynamic model of robot in the joint space as follows [54]

$$M(q)\ddot{q}+C(q,\dot{q})\dot{q}+G(q)=\tau+J^T(q)f, \tag{39}$$

where q, $\dot{q}$, $\ddot{q}\in\mathbb{R}^m$ are the joint angular displacement, velocity and acceleration vectors, respectively. $M(q)\in\mathbb{R}^{m\times m}$ is the symmetric and positive definite inertia matrix, $C(q,\dot{q})\dot{q}\in\mathbb{R}^m$ is the vector of Coriolis and centripetal force, $G(q)\in\mathbb{R}^m$ denotes the vector of the gravitational force. $\tau\in\mathbb{R}^m$ denotes the vector of the control input torque, $f\in\mathbb{R}^n$ is the vector of the interaction force generated by the human partner, $J(q)\in\mathbb{R}^{n\times m}$ is the Jacobian matrix, where n denotes the dimension in the Cartesian space. The forward kinematics of the robot is given by $x=\Phi(q)$, differentiating which with respect to time results in $\dot{x}=J(q)\dot{q}$. Based on the inverse kinematics, the velocity vector $\dot{q}$ and the acceleration vector $\ddot{q}$ in the joint space can be described as

$$\begin{aligned}\dot{q} &= J^{-1}(q)\dot{x}\\ \ddot{q} &= \dot{J}^{-1}(q)\dot{x}+J^{-1}(q)\ddot{x},\end{aligned} \tag{40}$$

where $J^{-1}(q)$ denotes the pseudoinverse of $J(q)$. $M_t(x)\in\mathbb{R}^{n\times n}$, $C_t(x,\dot{x})\dot{x}\in\mathbb{R}^n$ and $G_t(x)\in\mathbb{R}^n$ in the Cartesian space in (1) can be calculated as

$$\begin{aligned}M_t(x) &= J^{-T}(q)M(q)J^{-1}(q)\\ C_t(x,\dot{x}) &= J^{-T}(q)(C(q,\dot{q})-M(q)J^{-1}(q)\dot{J}(q))J^{-1}(q)\\ G_t(x) &= J^{-T}(q)G(q)\\ u &= J^{-T}(q)\tau.\end{aligned} \tag{41}$$

In Section IV, we define m_r as the mass of link r, define l_r as the length of link r, and define l_{cr} as the distance from the mass center of link r to joint $r-1$, and define I_r as the moment of Inertia of link r. The simulation parameter values are chosen as: m_1=2.0kg, m_2=0.85kg, l_1=1.40m, l_2=1.24m, l_{c1}=0.70m, l_{c2}=0.62m, I_1=0.980kgm^2, I_2=0.953kgm^2.

For simulations, dynamic model parameter matrices of robot $M(q)$, $C(q,\dot{q})$, $G(q)$ in the joint space in

(39) can be calculated as

$$M(q) = \begin{bmatrix} m_{t1} & m_{t2} \\ m_{t3} & r(2) \end{bmatrix} \tag{42}$$

$$C(q,\dot{q}) = \begin{bmatrix} c_{t1} & c_{t2} \\ c_{t3} & 0 \end{bmatrix} \tag{43}$$

$$G(q) = \begin{bmatrix} g_{t1} \\ g_{t2} \end{bmatrix}, \tag{44}$$

where $m_{t1} = r(1) + r(2) + 2r(3)\cos(q(3))$, $m_{t2} = r(2) + r(3)\cos(q(3))$, $m_{t3} = r(2) + r(3)\cos(q(3))$, $c_{t1} = -r(3)q(4)\sin(q(3))$, $c_{t2} = -r(3)(q(2) + q(4))\sin(q(3))$, $c_{t3} = r(3)q(2)\sin(q(3))$, $g_{t1} = r(4)g\cos(q(1)) + r(5)g\cos(q(1) + q(3))$, $g_{t2} = r(5)g\cos(q(1) + q(3))$, where the system state variables $q = [q(1); q(3)]$, $\dot{q} = [q(2); q(4)]$, $q(1)$ and $q(3)$ denote first and second joint angle, respectively, $q(2)$ and $q(4)$ denote first and second joint angular velocity, respectively, the variables $r(1) = m_1 l_{c1}^2 + m_2 l_1^2 + I_1$, $r(2) = m_2 l_{c2}^2 + I_2$, $r(3) = m_2 l_1 l_{c2}$, $r(4) = m_1 l_{c2} + m_2 l_1$ and $r(5) = m_2 l_{c2}$. The Jacobian matrix in (39) can be obtained according to l_1, l_2 and q as follows

$$J = \begin{bmatrix} J_{11} & J_{12} \\ J_{21} & J_{22} \end{bmatrix}, \tag{45}$$

where $J_{11} = -l_1\sin(q(1)) - l_2\sin(q(1) + q(3))$, $J_{12} = -l_2\sin(q(1) + q(3))$, $J_{21} = l_1\cos(q(1)) + l_2\cos(q(1) + q(3))$, $J_{22} = l_2\cos(q(1) + q(3))$.

If we obtain $M(q)$, $C(q,\dot{q})$, $G(q)$ and J, we can calculate dynamic parameter matrices of robot in the Cartesian space $M_t(x)$, $C_t(x,\dot{x})$ and $G_t(x)$ based on (41).

IX. Appendix B

Some trivial derivations are described in this appendix. According to Eqs. (2), (7) and (8), we can obtain the partial derivative $\frac{\partial E_{Mi}}{\partial f_i}$, $\frac{\partial f_i}{\partial \hat{x}_{di}}$ and $\frac{\partial \hat{x}_{di}}{\partial \hat{\Theta}_i}$ as follows

$$\frac{\partial E_{Mi}}{\partial f_i} = f_i, \frac{\partial f_i}{\partial x_{di}} = K_{hi}, \frac{\partial \hat{x}_{di}}{\partial \hat{\Theta}_i} = S(n_i). \tag{46}$$

Then, Eq. (9) can be obtained.

From Eq. (13) we can obtain

$$\sum_{j=1}^{N} 2(-\hat{D}_h \dot{x}_{ij} + \hat{K}_h z_{ij} - f_{ij})(-\dot{x}_{ij}) = 0$$
$$\sum_{j=1}^{N} 2(-\hat{D}_h \dot{x}_{ij} + \hat{K}_h z_{ij} - f_{ij}) z_{ij} = 0. \tag{47}$$

which leads to

$$-\hat{D}_h \sum_{j=1}^{N} \dot{x}_{ij}^2 + \hat{K}_h \sum_{j=1}^{N} \dot{x}_{ij} z_{ij} - \sum_{j=1}^{N} \dot{x}_{ij} f_{ij} = 0$$
$$-\hat{D}_h \sum_{j=1}^{N} \dot{x}_{ij} z_{ij} + \hat{K}_h \sum_{j=1}^{N} z_{ij}^2 - \sum_{j=1}^{N} z_{ij} f_{ij} = 0. \tag{48}$$

Then, we can obtain estimates $\hat{D}_h$ and $\hat{K}_h$ by solving the above two equations:

$$\begin{bmatrix} \hat{D}_h \\ \hat{K}_h \end{bmatrix} = \begin{bmatrix} -\sum_{j=1}^{N} \dot{x}_{ij}^2 & \sum_{j=1}^{N} \dot{x}_{ij} z_{ij} \\ -\sum_{j=1}^{N} z_{ij} \dot{x}_{ij} & \sum_{j=1}^{N} z_{ij}^2 \end{bmatrix}^{-1} \times \begin{bmatrix} \sum_{j=1}^{N} \dot{x}_{ij} f_{ij} \\ \sum_{j=1}^{N} z_{ij} f_{ij} \end{bmatrix}. \tag{49}$$

According to the moving average algorithm, we can obtain (14).